

Analysis and Design of a Quasi-TEM Slotted Tube Resonator for UHF-MRI

Kamila Aliane¹, Nadia Benabdallah², Nasreddine Benahmed¹,
Rachid Bouhmidj¹ and Fethi Tarik Bendimerad¹

¹Department of Telecommunications, University Abou Bekr Belkaid-Tlemcen,

²Department of Physics, Preparatory School of Sciences and Technology (EPST-Tlemcen),
Tlemcen, Algeria

ABSTRACT

Using the finite element method (FEM) and method of moments (MoM) in two dimensions, the electromagnetic (EM) analysis and design of a quasi-TEM slotted tube resonator (STR) are presented. The modeling of this resonator consists in analyzing the even- and odd-mode characteristic impedances (Z_{0e} , Z_{0o}), effective dielectric constants (ϵ_{effe} , ϵ_{effo}), the primary inductive and capacitive matrices ([L], [C]) and simulates the frequency response of S_{11} at the RF port of the designed inhomogeneous MRI probe using transmission line method (TLM). As an application, we present the design results of a UHF-MRI probe loaded with a human head model of average relative dielectric constant of 64 and using the optimum configuration of the TEM STR. The probe with high Q operates at 340 MHz (proton imaging at 8 T) and has -130.6 dB minimum reflections. The UHF-MRI probe using quasi-TEM STR is easy to construct, inexpensive, and simple to operate. Furthermore, the coil presented here may be constructed to work at different resonances frequencies.

Keywords - Biological load, EM-parameters, high Q, frequency response, FEM, MoM and TLM calculations, human head model, Quasi-TEM slotted tube resonator, S-parameters, UHF-MRI probe.

I. INTRODUCTION

Magnetic resonance imaging (MRI) is widely used to obtain clear images inside human body, especially high water content tissues such as muscle, brain etc. The fundamental principle of MRI is to receive nuclear magnetic resonance signals induced by radiating electromagnetic (EM) wave pulse to human body which is placed inside the high intensity static magnetic field. MRI is a method that has been developed by Lauterbur [1], Mansfield and Grannell [2] and is based on the knowledge of nuclear magnetic resonance (NMR) technique. The 2003 Nobel Prize in physiology or medicine was awarded to these scientists responsible for the development of nuclear magnetic resonance as an imaging technique. MRI has since become a standard clinical method.

The MRI system is composed of various elements including radio frequency (RF) coil, which plays an essential role in imaging. Several types of RF coils, such as saddle coil [3], transverse electromagnetic birdcage coil resonator (TEM

BCR) [4-5], TEM slotted elliptical tube resonator (TEM SER) [6-9] and TEM slotted tube resonator (TEM STR) [10-11] have been developed to use for different usages. Among these RF coils, the TEM STR has gradually come to be employed since it can produce the uniform magnetic field and can suppress the electric field.

This article is a continuation of our previous paper that appeared in Physics in Medicine and Biology magazine [12]. In support of the analysis and design of a high-Q quasi-TEM resonator for UHF-MRI applications based on loaded slotted tube resonator, we developed effective approaches based on the use of the finite element method (FEM) and the method of moments (MoM).

For this type of quasi-TEM resonator, there are no numerical or experimental results in the scientific literature. For this reason we were obliged, for the same geometrical and physical parameters of our quasi-TEM resonator, to make simulations by using our two numerical approaches (FEM and MoM).

The aim of this work is to determine, for the optimum configuration of the quasi-TEM STR, the even- and odd-mode characteristic impedances (Z_{0e} , Z_{0o}), effective dielectric constants (ϵ_{effe} , ϵ_{effo}), the primary inductive and capacitive matrices ([L], [C]) and simulates the frequency response of S_{11} at the RF port of the designed loaded UHF-MRI probe using transmission line method (TLM) [13].

To demonstrate our numerical methods, the design results of a quasi-TEM MRI probe with high Q and -130.6 dB minimum reflection loaded with a human head model of average relative dielectric constant of $\epsilon_r=64$ [14] for proton imaging at 8 T (340 MHz) will be presented.

II. QUASI-TEM SLOTTED TUBE RESONATOR

The quasi-TEM slotted-tube resonator is schematically shown in Fig. 1-a. This coil is assumed to be lossless and consists of two conductive sheets, containing the biological load of dielectric constant ϵ_r , t thick carrying opposite currents on each side of an inner cylinder of radius r_c . The conductive sheets are connected at the ends with capacitors to the cylindrical outer shield of radius r_b (Fig. 2).

The cross section of the quasi-TEM STR is presented in Fig. 1-b. The angle θ is called the "window angle". The quasi-TEM STR structure generally performs as well as inhomogeneous cylindrical birdcage coils, with the advantages of being easier to construct and operate. In reference [12], we have shown that for $r_b=2.4r_c$ and $t=0.2r_c$, the optimum field homogeneity for an unloaded

slotted tube resonator (i.e. TEM STR) is obtained for a window angle of 60°. Unfortunately changes introduced by human biological loads with high dielectric constants in the quasi-TEM resonator are not negligible, because of the non homogeneity of the structure. For this reason we adapted our previous numerical tools based on FEM and MoM approaches used in [12] to analyze slotted tube resonator loaded with biological elements.

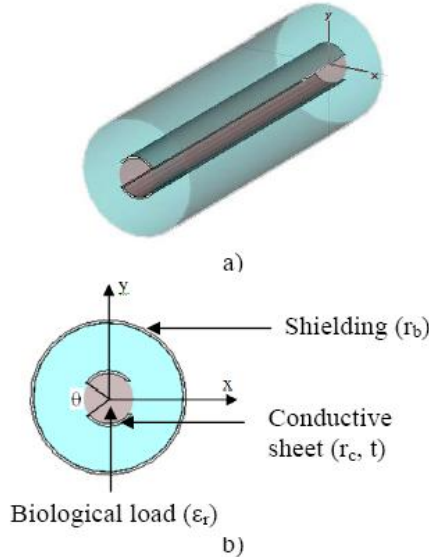


Fig. 1. (a) Quasi-TEM slotted tube resonator and (b) Cross section of the quasi-TEM STR.

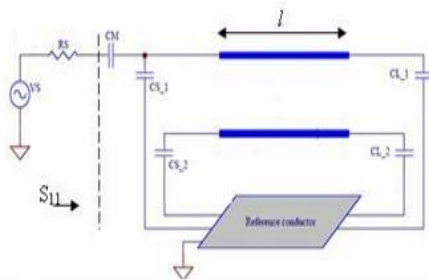


Fig. 2. Schematic circuit of the UHF-MRI probe using quasi-TEM STR resonator.

III. EM-PARAMETERS OF THE QUASI-TEM STR

The electromagnetic properties of the quasi-TEM slotted-tube resonator can be described in terms of its primary parameters [L], [C] and its secondary parameters: the even- and odd-mode characteristic impedances (Z_{0e}, Z_{0o}), effective dielectric constants (ε_{effe}, ε_{effo}), and the loaded quality factor Q.

where:

$$[L] = \begin{bmatrix} L_{11} & L_{12} \\ L_{21} & L_{22} \end{bmatrix} \quad [C] = \begin{bmatrix} C_{11} & C_{12} \\ C_{21} & C_{22} \end{bmatrix}$$

The inductance matrix [L] contains the self-inductances of the sheets on the diagonal, and the mutual inductances between sheets in the off-diagonal terms.

Matrix [C] accounts for the capacitive effects between the two conductive sheets, characterizing the electric field energy storage in the quasi-TEM STR.

The coefficients for these matrices are obtained by solving a two-dimensional static field problem using FEM [15-16] and MoM methods [17].

For the FEM approach and under FreeFEM environment [18], the solution is obtained by solving the Laplace’s equation (Fig. 3-a):

$$div [\epsilon_r \nabla_i V(x, y)] = 0 \tag{1}$$

subject to:

V = 1 volt on the ith conductor’s surface.

V = 0 on all others conductors.

This solution represents the distribution of the potential V at the different mesh nodes of the structure (Fig. 3-b).

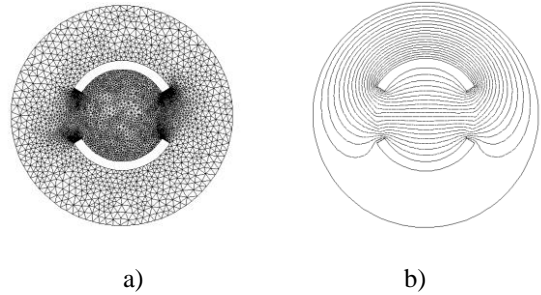


Fig. 3. FEM meshes on (a) and potential distribution on (b).

When the potential V is known, we calculate the ith row of the [C] matrix from the electric charge on each conductor.

$$C_{ij} = \frac{1}{V_0} \oint_{l_j} q_s dl \tag{2}$$

Where V₀=1volt, q_s=ε₀ε_rE_N, l_j represents the contour around the jth conductor and E_N is the normal component of the electric field.

In the high-frequency limit, i.e. the skin depth is sufficiently small such that current flow occurs only on the surface of the conductors, the inductance matrix [L] can be obtained from the matrix [C₀] [12]. The inductance matrix in terms of [C₀] calculated for (ε_r = 1) is:

$$[L] = \mu_0 \epsilon_0 [C_0]^{-1} \tag{3}$$

For the MoM approach, the numerical calculations of the EM-parameters of the studied resonator were carried out with LINPAR for windows (Matrix Parameters for Multiconductor Transmission Lines), a 2D software for numerical evaluation of the quasi static matrices for multiconductor transmission lines embedded in piecewise-homogeneous dielectrics [17]. The technique used in the program is based on an electrostatic analysis. In this analysis the dielectrics are replaced by bound charges in a vacuum, and the conducting bodies are replaced by free charges. A set of integral equations is derived for the charge distribution from the boundary conditions for the electrostatic potential and the normal component of the electric field. The method of moments is applied to these equations, with a piecewise-constant (pulse) approximation for the total charge density and the Galerkin technique. LINPAR for windows can analyse arbitrary planar transmission lines and can also analyse any other structure defined by the user.

For our slotted tube-line quasi-TEM resonator, we were obliged to supply the cross section of the structure and all relevant dielectrics characteristics including the segmentation by using our programs in FORTRAN (Figure 4).

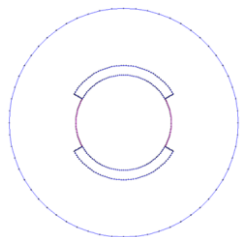


Fig. 4. Segmentation of the charged surfaces of the slotted tube-line quasi-TEM resonator.

When the EM-parameters are determined, it is possible to estimate the resonance spectrum (S_{11}) of the resonator shown in Fig. 2 using our programs based on the transmission line method (TLM).

The MRI probe developed for this article consists of the STR resonator with length l , matching capacitor C_M , and terminating capacitors C_{Si} and C_{Li} ($i=1, 2$).

The loaded quality factor (Q) of the quasi-TEM resonator can be estimated from the reflection-parameter (S_{11}) sweep with frequency [12]:

$$Q = \frac{f_r}{f_u - f_l} \quad (4)$$

where

f_r =the resonance frequency of the circuit,

f_u =3-dB frequency above the resonance frequency, and

f_l =the 3-dB frequency below the resonance frequency.

IV. RESULTS

We applied our modified and coherent FEM and MoM-based numerical tools to the analysis and design of an MRI resonator using quasi-TEM STR. The FEM and MoM approaches make it possible to simulate the performance of a design and decide if a given set of constraints makes it possible to realize the UHF-probe.

To design a loaded MRI probe operating at 8 Tesla (i.e 340 MHz) and using the optimum configuration of the TEM STR (for $\theta=60^\circ$), we analyzed the structure shown in figure 2 with the following set of features:

an inner cylinder radius (r_c) of 36.83mm;

a sheet thickness (t) of (0.2 r_c); and

biological loads of dielectric constants ϵ_r listed in table 1 [19].

Table I: Load properties at 340 MHz.

Load type	ϵ_r [19]
Fat	5,14
Bone-Cortical	13,91
Bone-Cancellous	21,84
Nerve	36,80
White-Matter	41,85
Skin	43,07
Cartilage	44,82
Mixed-GM-WM	49,45
Dura	52,23
Mucosa	52,69
Cerebellum	54,40
Cornea	55,40
Gray-Matter	57,05
Blood	57,50
Tongue	59,64
Muscle	65,57
Vitreous-Humor	68,30
CSF	69,08

Our FEM and MoM approaches were employed as shown in figures 3 and 4 to determine the EM-parameters of the quasi-TEM resonator. As discussed above, the integration of the normal flux over the conductor contours determines the per-unit-length parameter matrices. For instance, table 2 lists the elements of the [L] and [C] matrices for $\epsilon_r=65.57$. This table shows clearly the good coherence between the results obtained by our two numerical approaches for inhomogeneous slotted tube-line.

Table II: Primary EM-parameters of inhomogeneous STR loaded with a biological element of a dielectric constant of 65.57

	$C_{11}=C_{22}$ (pF/m)	$C_{12}=C_{21}$ (pF/m)	$L_{11}=L_{22}$ (nH/m)	$L_{12}=L_{21}$ (nH/m)
FEM	778.9	-723.7	233.0	62.04
MoM	781.1	-743.0	234.4	66.04

In table 3, we present the influence of the dielectric constants ϵ_r at 340 MHz of the biological load on the EM-parameters of the slotted tube-line quasi-TEM resonator. This table with the results obtained for the elements of the matrix [L] listed into table 2 and which does not vary with the biological properties, are essential for the design of inhomogeneous MRI probes operating at 8 T.

First, we designed a MRI probe using unloaded slotted tube-line TEM resonator with the following features: a resonator length, l (with respect to the wavelength in free space λ_0), of 22 cm ($l=0.25 \lambda_0$); a matching capacitor, C_M , with value of 28.63 pF, and source and load terminating capacitors, C_S and C_L , respectively, both with value of 1.38 pF.

For the same length (i.e. $l=22$ cm) of the unloaded MRI probe, we introduced a given biological load with a

dielectric constant (ϵ_r) of table 1 into the MRI resonator and we tuned the matching capacitor C_M , and the terminating capacitors C_{Si} and C_{Li} until resonance. At 340 MHz, the obtained values of these capacitors are given in table 4 for each biological load.

From this table, it appears clearly that the value of the matching capacitor varies between 20 and 30 pF, whereas the value of the source and load terminating capacitors varies between 1 and 2 pF for MRI experiences using the optimum configuration of quasi-TEM STR.

Finally, the simulated frequency responses of S_{11} at the RF port for the designed MRI probe using both an unloaded TEM resonator and a quasi-TEM STR with dielectric constant ϵ_r of 65.57 (for example) are shown in figure 5 using both our programs (TLM) and MATPAR software [20]. Table 5 lists the values of the S_{11} -parameter for MRI probes designed to operate at 340 MHz with and without the biological load.

From figure 5, it appears that the results obtained from our programs using TLM are in very good agreement with those obtained using MATPAR software. Furthermore the biological load introduced into the STR improves the value of the reverse transmission, S_{11} at 340 MHz. Using Eq. 4, Q was estimated to be very superior to 500.

Table IV: Values of the matching (C_M), source (C_S) and load (C_L) terminating capacitors at resonance for MRI experiences using STR.

Load type	C_M (pF)	$C_{Si} = C_{Li}$ (pF)
Air	28.63	1.38
Fat	20.0	1.00
Bone-Cortical	30.0	2.00
Bone-Cancellous	27.5	1.80
Nerve	20.7	1.10
White-Matter	20.0	1.00
Skin	20.0	1.00
Cartilage	30.0	1.00
Mixed-GM-WM	30.0	2.00
Dura	30.0	2.00
Mucosa	30.0	2.00
Cerebellum	30.0	2.00
Cornea	30.0	2.00
Gray-Matter	29.6	2.00
Blood	29.5	1.99
Tongue	29.24	1.91
Muscle	29.86	1.71
Vitreous-Humor	28.1	1.67
CSF	28.82	1.67

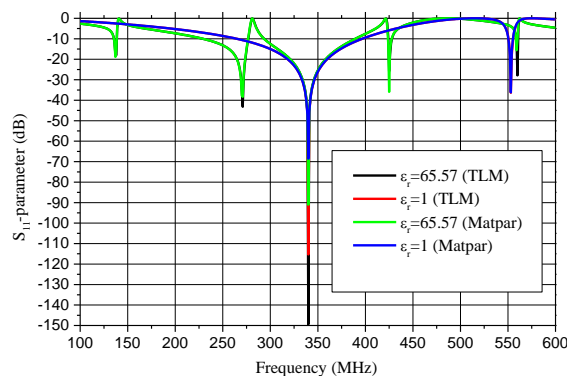


Fig. 5. Reverse transmission, S_{11} , at the RF port of the designed high Q MRI probe using STR.

Table V: S_{11} -parameter obtained using TLM and MATPAR software.

	S_{11} from TLM (dB)	S_{11} from MATPAR (dB)
TEM STR	-115,30	-68,55
Quasi-TEM STR	-149,42	-91,02

All the numerical results shown into this paper were obtained while considering only one biological element which filled completely the quasi-TEM STR volume for the following geometrical parameters:

- a given inner cylinder radius (r_c);
- a sheet thickness (t) of $(0.2 r_c)$;
- a window angle (θ) of 60° ; and
- a resonator length, l (with respect to the wavelength in free space λ_0), of 22 cm ($l=0.25\lambda_0$).

In practice for UHF-MRI proton imaging at 8 T these results remain always valid when the quasi-TEM STR is filled by inhomogeneous biological load (like human head).

In reference [14], 18 tissue types, in addition to air, were identified in the images given in figure 6 in order to obtain a detailed human head structure. These included: blood, bone-cancellous, bone-cortical, cartilage, cerebellum, cornea, cerebro spinal fluid (CSF), dura, fat, gray-matter (GM), mucosa, muscle, nerve, skin, tongue, vitreous-humor, white-matter (WM), and mixed-GM-WM.

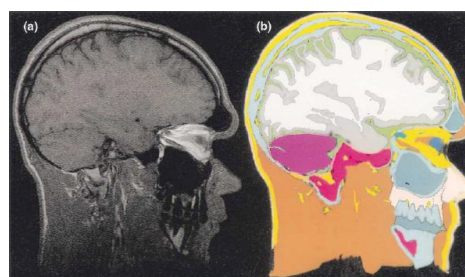


Fig. 6. (a) An MRI image (b) its equivalent anatomically detailed human head model used in [14].

If we consider that the average relative dielectric constant of the human head is 64 [14], then the wavelength inside the head is approximately 11 cm. As a result, the EM-parameters of the quasi-TEM STR loaded with the human head model obtained from our MoM analyses include even- and odd-mode characteristic impedances (Z_{0e} , Z_{0o}) of 88.76 Ω and 10.64 Ω , effective dielectric constants (ϵ_{effe} , ϵ_{effo}) of 1.03 and 22.53 and primary inductive and capacitive matrices ($[L]$, $[C]$) as follows:

$$[L] = \begin{bmatrix} 234.4 & 66.04 \\ 66.04 & 234.4 \end{bmatrix} \left(\frac{nH}{m} \right);$$

$$[C] = \begin{bmatrix} 763.4 & -725.2 \\ -725.2 & 763.4 \end{bmatrix} \left(\frac{pF}{m} \right).$$

Figure 7 presents the simulated frequency responses of S_{11} at the RF port of the UHF-MRI probe using quasi-TEM STR loaded with the human head model. For matching capacitor C_M of 29.8 pF and terminating capacitors C_{Si} and C_{Li} both of 1.75 pF, the probe operates at 340 MHz (proton imaging at 8 T) and has -130.6 dB minimum reflections.

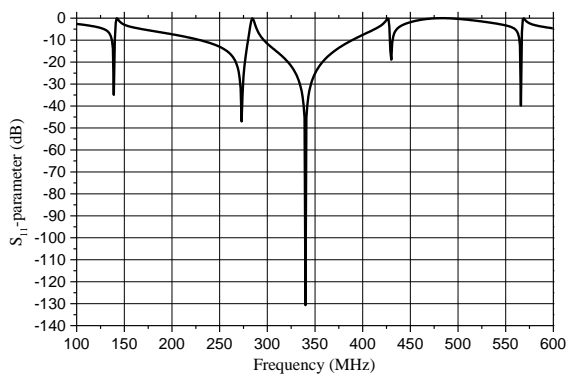


Fig. 7. Reverse transmission, S_{11} , at the RF port of the UHF-MRI probe using quasi-TEM STR loaded with the human head model.

V. CONCLUSION

This article presents the analysis and the design of UHF-MRI probe with high Q, operating at 8 T (i.e. 340 MHz) and using the optimum configuration of the slotted tube-line quasi-TEM resonator.

A finite element method and a method of moments programs have been adapted and employed to accurately characterize the even- and odd-mode characteristic impedances (Z_{0e} , Z_{0o}), effective dielectric constants (ϵ_{effe} , ϵ_{effo}), the primary inductive and capacitive matrices ($[L]$, $[C]$) of the loaded MRI resonator.

These EM parameters of the slotted tube-line can be also used for the design of other microwave components like couplers.

When the EM-parameters have been determined, it is possible to simulate the frequency response of S_{11} at the RF port of the designed quasi-TEM resonator loaded with any biological element.

The quasi-TEM UHF-MRI probe with high Q, operating at

340 MHz and using STR loaded with a human head model of average relative dielectric constant of 64, has -130.6 dB minimum reflections and is easy to construct, inexpensive, and simple to operate.

In addition, the quasi-TEM STR presented here may be constructed to work at different resonances frequencies.

REFERENCES

- [1] PC Lauterbur, Image formation by induced local interactions: examples employing nuclear magnetic resonance, *Nature*, 242, 1973, 190-191.
- [2] P. Mansfield, PK. Grannell, NMR diffraction in solids?, *J. Phys.* 1973, C 6: L422-L426.
- [3] C. E. Garrido Salmon, E. L. G'ea Vidoto, M. J. Martins and A. Tann'us, Optimization of Saddle Coils for Magnetic Resonance Imaging, *Brazilian Journal of Physics*, 36(1A), 2006, 4-8.
- [4] G. Bogdanov and R. Ludwig, A Coupled Microstrip Line Transverse Electromagnetic Resonator Model For High-Field, *Magn. Reson. Med.*, 47, 2002, vol. 47, pp. 579-593.
- [5] R. Ludwi, G. Bodgdanov, J. King, A. Allard, and C.F. Ferris, A dual RF resonator system for high-field functional magnetic resonance imaging of small animals, *Journal of Neuroscience Methods*, 132, 2004, 125-135.
- [6] S. Crozier, LK. Forbes, WU. Roffmann, K. Luescher and DM. Doddrell, A methodology for current density calculations in high-frequency RF resonators, *Concepts Magnetic Resonance*, 9, 1997, 195-210.
- [7] MC. Leifer, Theory of the quadrature elliptic birdcage coil, *Journal of Magnetic Resonance Medicine*, 38, 1997, 726-732.
- [8] S. Bobrof and MJ. McCarth, Variations on the slotted-tube resonator: Rectangular and elliptical coils, *Journal of Magnetic Resonance Imaging*, 17, 1999, 783-789.
- [9] N. Benabdallah, N. Benahmed and B. Benyoucef, Analyzing a resonator for MRI applications, *Microwaves and RF*, 46(11), 2007, 92-98.
- [10] D. W. Alderman and D. M. Grant, An efficient decoupler coil design which reduces heating in conductive samples in superconducting spectrometers, *J. Magn. Reson.*, 34, 1979, 425-433.
- [11] S. Li, Q.X. Yang, M.B. Smith, RF coil optimization: Evaluation of B1 field homogeneity using field histograms and finite element calculations, *Mag. Reson. Imaging*, 1994, vol. 12, pp. 1079-1087.
- [12] N. Benabdallah, N. Benahmed, B. Benyoucef, R. Bouhmidi and M' Khelif, EM analysis of the slotted-tube resonator with circular cross section for MRI applications, *Journal of Physics in Medicine and Biology*, 52, 2007, 4943-4952.
- [13] R. P. Clayton, *Analysis of Multiconductor Transmission Lines* (New York: John Wiley, 2008).
- [14] T.S. Ibrahim, R. Lee, B. A. Baertlein, A. M. Abduljalil, H. Zhu and P. L. Robitaille, Effect of RF coil excitation on field inhomogeneity at ultra high fields: A field optimized TEM resonator, *Mag. Res. Imag.*, 19, 2001, 1339-1347.
- [15] R. Bouhmidi, N. Benabdallah, N. Benahmed and M'. Khelif, Design coupled microstrip resonators for MRI, *Microwaves and RF*, 46(3), 2007, 59-66.

- [16] N. Ben Ahmed, M. Feham, and M. Khelif, Analysis and design of a coupled coaxial line TEM resonator for magnetic resonance imaging, *Journal of Physics in Medicine and Biology*, 51, 2006, 2093-2099.
- [17] A.R. Djordjevic, D. Darco, M.C. Goran, T.K. Sarkan, *Circuit Analysis Models for Multiconductors Transmission Lines* (Artech House, 1997).
- [18] www.Freefem.org
- [19] C. Gabriel, *Compilation of dielectric properties of body tissues at RF and microwave frequencies* (AL/OE-TR-1996-0037, 1996).
- [20] A.R. Djordjevic, M. Bazdar, G. Vitosevic, T. Sarkar, and R. F. Harrington, *Scattering parameters of microwave networks with multiconductor transmission lines* (Artech House, Norwood, MA, 1990).

Table III: EM-parameters of the quasi-TEM STR at 340 MHz.

Load type	ϵ_r	ϵ_{eff0}	ϵ_{eff0}	$Z_{0e}(\Omega)$	$Z_{0o}(\Omega)$	$C_{11}=C_{22}$ (pF/m)	$C_{12}=C_{21}$ (pF/m)
Air	1	1	1	90.11	50.47	51.51	-14.54
Fat	5,14	1.02	2.42	89.21	32.44	98.9	-61.13
Bone-Cortical	13,91	1.026	5.42	88.92	21.68	198.1	-160.1
Bone-Cancellous	21,84	1.028	8.13	88.85	17.71	287.6	-249.5
Nerve	36,80	1.029	13.24	88.80	13.87	456.4	-418.3
White-Matter	41,85	1.029	14.96	88.79	13.05	513.4	-475.3
Skin	43,07	1.029	15.38	88.78	12.87	527.2	-489.1
Cartilage	44,82	1.03	15.98	88.78	12.63	546.9	-508.8
Mixed-GM-WM	49,45	1.03	17.56	88.78	12.05	599.2	-561.1
Dura	52,23	1.03	18.51	88.77	11.73	630.6	-592.4
Mucosa	52,69	1.03	18.67	88.77	11.68	635.8	-597.6
Cerebellum	54,40	1.03	19.25	88.77	11.51	655.1	-616.9
Cornea	55,40	1.03	19.59	88.77	11.41	666.3	-628.2
Gray-Matter	57,05	1.03	20.15	88.77	11.24	685.0	-646.8
Blood	57,50	1.03	20.31	88.77	11.20	690.0	-651.9
Tongue	59,64	1.03	21.04	88.76	11.01	714.2	-676.0
Muscle	65,57	1.03	23.06	88.76	10.51	781.1	-743.0
Vitreous-Humor	68,30	1.03	24.0	88.76	10.31	811.9	-773.8
CSF	69,08	1.03	24.26	88.76	10.25	820.7	-782.6